Photochemical Synthesis of Ultrafine Cubic Boron Nitride Nanoparticles under Ambient Conditions**

Hui Liu, Peng Jin, Yan-Ming Xue, Cunku Dong, Xiang Li, Cheng-Chun Tang, and Xi-Wen Du**

Abstract: *Cubic boron nitride (c-BN) is a super-hard material whose hardness increases dramatically with decreasing size. However, c-BN nanoparticles (NPs) with sizes less than 10 nm have never been obtained. Herein we report a simple strategy towards the synthesis of ultrafine c-BN NPs with an average size of 3.5 nm. The method, under ambient conditions, exploits a laser-induced photochemical effect and employs dioxane solution of ammonia borane (AB) as a liquid target. Meanwhile, total dehydrogenation of AB is realized by laser irradiation. Therefore, this approach shows great potential for the preparation of super-hard NPs as well as controllable dehydrogenation.*

C-BN, known as the hardest material with thermal and chemical stability superior to diamond, has been widely applied in abrasives, cutting tools, and refractory fields,[1] and its hardness was proved to increase dramatically with the reduced particle size following the Hall–Petch relationship.[1e] However, c-BN is stable only at high pressure, and c-BN NPs smaller than 10 nm have not yet been reported owing to the rapid growth of nuclei under the fierce synthetic conditions which involve high temperature and high pressure.[1,2] Therefore, it is of interest to explore an effective strategy toward ultrafine c-BN NPs.

The popular techniques for the synthesis of c-BN can be classified into three categories, namely, phase transformation, solvothermal reaction, and laser ablation.[1–3] The phase transformation of a graphite-like or amorphous BN precursor is usually conducted under high pressures (several tens GPa) and high temperatures (1300–2000 K),[1,2] and the smallest c-BN NPs by this approach have an average size of 14 nm, prepared at 20 GPa and 1770 K.[1a,3d] Solvothermal reactions can generate a large amount of c-BN materials, however, the NPs produced usually have large sizes of more than 30 nm.[3a,c] In comparison with these methods, laser ablation is a facile

method to synthesize nanostructures with complex morphologies,[4] metastable phases,[5] and novel properties.[4a,b, 5b, 6] Particularly, pulsed laser ablation has proved its reliability for the synthesis of NPs.[7] For the preparation of c-BN, a high-energy pulsed laser was employed to stimulate a hexagonal BN target in acetone.[3b] The high-energy laser generated a plasma plume with high temperature and high pressure in which species condensed and grew up at a very high rate, giving rising to large c-BN NPs (> 10 nm).[3b] In addition, liquid targets, including suspensions with particles and solution with precursors,[8] are also used in laser ablation, and unusual photochemical or thermochemical reactions are expected to happen under the high-energy laser irradiation, which can produce novel materials at rather large scale.[9]

Considering the unique advantages of laser ablation of a liquid target, herein we choose AB as the precursor, which has been employed for the synthesis of BN materials.[10] After the dioxane solution of AB was irradiated with a pulsed laser, c-BN NPs were obtained with an average size of 3.5 nm, which is the smallest size ever reported. The experimental and calculated results indicates the six hydrogen atoms in an AB molecule can be simultaneously removed during a laser pulse, which is totally different from the stepwise elimination of hydrogen atoms and formation of intermediate impurities in solvothermal synthesis. In particular, the solvent and laser energy were found to be critical for the breakage of chemical bonds. To our knowledge, this is the first report on preparing c-BN NPs at ambient temperature and pressure, and our work paves a facile way to the mass production of ultrafine c-BN NPs which may have a very high hardness in accord with the Hall–Petch relationship. Moreover, laser irradiation can release the hydrogen in AB completely at one time, demonstrating an efficient and controllable dehydrogenation from hydrogen storage material.

After the dioxane solution of AB was irradiated under ambient conditions by a nanosecond laser (that is, one that delivers laser irradiation in nanosecond-long pulses) with a wavelength of 1064 nm for 10 min, the solution temperature was kept constant, and a large amount c-BN NPs were obtained in the solution (Figure 1a). A statistical analysis on more than 200 NPs in Figure 1a demonstrates that the as-prepared c-BN NPs are nearly monodisperse with diameters of 3.5 ± 0.6 nm ($\sigma = 17.1\%$; inset of Figure 1a). High-resolution transmission electron microscope (HRTEM) image in Figure 1b shows that the c-BN NPs usually have high density of twins and stacking faults, while monocrystal c-BN NPs were also found in the product (Figure S1a in the Supporting Information). The selected area electron diffraction pattern (SAED; Figure 1c) of the NPs agrees well with the cubic structure of bulk BN. Typical electron energy loss spectrum

[*] H. Liu, P. Jin, Y.-M. Xue, C.-C. Tang
Key Laboratory of Micro- and Nano-scale Boron Nitride Materials of Hebei Province, School of Materials Science and Engineering
Hebei University of Technology, Tianjin (China)

H. Liu, C. Dong, X. Li, X.-W. Du
Institute of New-Energy Materials, Tianjin Key Laboratory of Composite and Functional Materials, School of Materials Science and Engineering, Tianjin University
No. 92 Weijin Road, Nankai District, Tianjin 300072 (China)
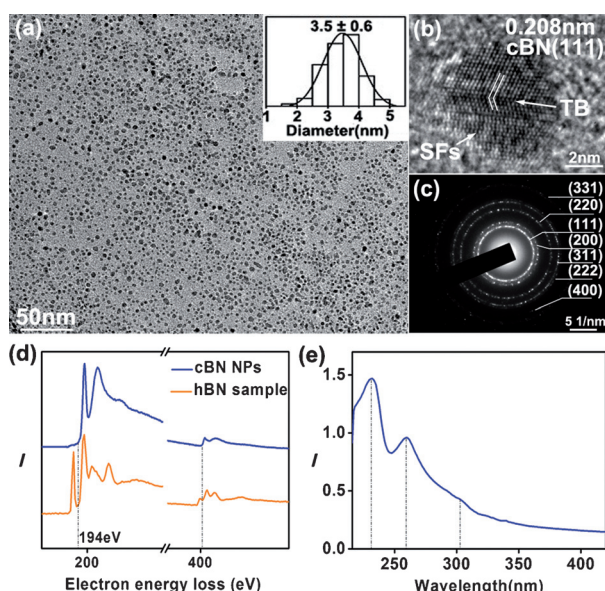E-mail: xwdu@tju.edu.cn

Figure 1. c-BN NPs synthesized at room temperature by ns pulse laser irradiation of dioxane solution of AB. a) TEM image. Inset: a size histogram and corresponding Gaussian fit. b) HRTEM image of a c-BN nanoparticle, TB = twin boundary, SFs = stacking faults. c) Selected area electron diffraction pattern, d) EELS spectrum of c-BN NPs with that of an h-BN sample as a reference, e) Absorption spectrum of c-BN.

Figure 2. a) FTIR spectrum of AB, dioxane, and dioxane solution of AB before and after laser irradiation, b) Theoretical optimized geometry of the complex formed between an AB and three dioxane molecules visualized using the CYLview software (dotted lines indicate hydrogen bonds, interatomic distances in Å).

(EELS) of the NPs shown in Figure 1d is consistent with the profile reported in literature.[2] Namely, the spectrum only exhibits single peak for the B-K and N-K edge of c-BN with onsets at 194 and 402 eV, respectively, and does not display the sp^2-hybridized peak arising from the transitions of the 1s electrons to the empty π^* antibonding orbitals. Energy dispersive spectrum (EDS) and X-ray diffraction (XRD) result shown in Figure S1b and S1c also confirm the formation of c-BN. The absorption spectrum of the suspension of c-BN in water suspension of c-BN in water reveals two distinct peaks (Figure 1e), the peak at 230 nm may be attributed to c-BN NPs with many stacking faults, while the peaks around 260 nm are attributed to the impurity or defect-related bands.[11] As hydrogen gas is formed as a byproduct during the photochemical synthesis of c-BN NPs. As shown in gas chromatography spectrum (Figure S2), two peaks at 40 and 50 s could be appointed to carrier Ar gas and H_2 gas, respectively, and the yield rate of hydrogen gas was estimated as 2.52 mmol h^{-1} (see the details in Part S3 and Figure S3 of the Supporting Information). In contrast, the hydrogen peak cannot be detected in the sample without laser irradiation.

To understand the formation mechanism of the c-BN NPs, we first investigated the intrinsic structure of the liquid target. Fourier transform-infrared spectrum (FTIR) was employed to analyze the molecular interaction. As shown in Figure 2a, after AB was dissolved in dioxane, the B–H stretching vibration peaks at 2387, 2343, and 2284 cm^{-1} shifted to 2378, 2322, and 2278 cm^{-1}, respectively, and the N–H stretching vibration peaks at 3315 and 3251 cm^{-1} shifted to 3307 and 3236 cm^{-1}, respectively. The blueshift may originate from the elongation of the B–H and N–H bonds, which was confirmed by the theoretical calculation (Figure 2b). The calculation
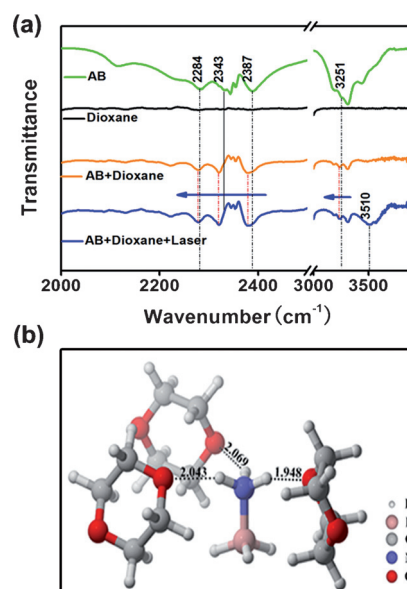
based on density functional theory (DFT; see details in Experimental Section) illustrates that an AB molecule favors formation of a stable complex (named as basic unit) with three dioxane molecules through N–H(AB)···O(dioxane) intermolecular hydrogen bonds (Figure 2b). The binding preference can be understood by considering the charge distributions of AB and dioxane: the positively charged hydrogen atoms at the NH_3 end of AB prefers to bond with the electron-rich oxygen atoms of dioxane, whereas the negatively charged hydrogen atoms at the BH_3 end do not favor the oxygen binding because of strong Coulomb repulsion. Compared with the isolated AB, the X–H (X = B, N) and the B–N bonds of the AB moiety in the complex are slightly elongated (B–H from 1.210 to average 1.216 Å; N–H from 1.017 to average 1.024 Å) and shortened (B–N from 1.661 to 1.631 Å), respectively, agreeing well with the FTIR results. Therefore, the interaction of AB with dioxane molecules strengthens the B–N bonds and weakens the X–H bonds, making the dehydrogenation of AB feasible. Moreover, a broad peak around 3510 cm^{-1} appeared in the spectrum of the sample after laser irradiation (blue line in Figure 2a), which arises from the moisture absorbed on the surface of the c-BN NPs,[3a] verifying the formation of c-BN NPs.

We then measured the light absorption of the liquid target which is an essential property for laser synthesis. As shown in the absorption spectra (Figure S4), AB, dioxane, and the dioxane solution of AB exhibit an strong absorption peak in the wavelength range of 1000–1100 nm, therefore, they can absorb the incident laser photons (wavelength 1064 nm) efficiently.

We further probed the influence of laser energy on the final product. At a high single-pulse energy (300 mJ), the product was composed of c-BN NPs (Figure 1a). As the

single-pulse energy decreased to 170 mJ, many amorphous nanoparticles were found to coexist with c-BN NPs (Figure S5a). Further turning the single-pulse energy down to 50 mJ resulted in completely amorphous NPs with diameters ranging from 15 to 100 nm (Figure S5b). The EDS mapping images in Figures S5d and S5e demonstrate that the amorphous NPs are composed of B and N. Similarly, large amorphous NPs emerged in the products obtained by using higher concentrations of AB (0.025 and 0.05 M), and their amount increased dramatically with the precursor concentration (Figure S6). Moreover, the amorphous structure could transform gradually into the hexagonal phase under the irradiation of electron beam in TEM (Figure S7a–d).

The crystal structure of bulk BN material depends on temperature and pressure. In the temperature–pressure phase diagram, hexagonal phase BN (h-BN) is stable at room temperature (298 K), while c-BN emerges only under external high pressure over 1.53 GPa (Figure 3). Nevertheless, the
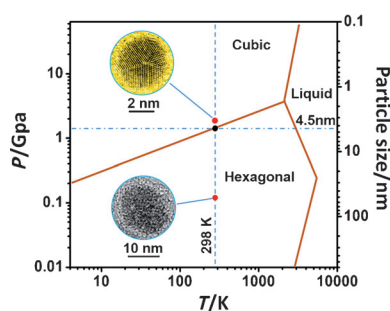

Figure 3. The temperature-pressure (particle size) phase diagram of BN. Inset: A c-BN nanoparticle with size of 3.5 nm (upper) and an amorphous BN nanoparticle with size of 16 nm (lower).

situation is considerably different when the dimensions of the BN material are reduced to the nanometer scale. The large surface curvature of fine NPs could cause an additional surface pressure (ΔP), and the correlation between the additional pressure and particle size followed the Laplace–Young equation [Eq (1)],

$$\Delta P = 4f/d \tag{1}$$

where d is the nanoparticle size, f a constant determined by the material type,[12] and the total pressure varied with the particle size by Equation (2)

$$P = 1 \text{ atm } + \Delta P = 0.101325 \text{ GPa } + 4f/d \tag{2}$$

As a result, the cubic phase can be stabilized in fine NPs even at ambient pressure and temperature. According to Equation (2), we extrapolated the pressure into particle size, and drew a vertical axis of particle size in the right of Figure 3, where the size threshold for achieving c-BN NPs at ambient conditions was determined as 4.5 nm (see details in Part S6 of the Supporting Information). The BN NPs obtained at high laser flux (300 mJ) have an average size of 3.5 nm which is smaller than the threshold value; hence it is natural for these NPs exist in the form of cubic phase at atmospheric pressure and room temperature.

We also tested three other solvents, pyridine, cyclohexane and water, to identify their capability in the photochemical synthesis of c-BN NPs. As shown in Figure S7, pyridine and cyclohexane can absorb laser light strongly. Although the clear absorption peak around 1064 nm is absent in the absorption spectrum of water, it absorbs the 1064 nm laser as reported by Zeng et al.[13] Likewise, FTIR spectra showed the redshift of the B−H stretching vibration peak when AB was dissolved in pyridine, but this phenomenon was not observed in the cyclohexane solution of AB (Figure S8), indicating pyridine could from basic units with AB, while cyclohexane could not owing to the lack of highly electronegative atoms. Considering the high solubility of AB in water, we believed that similar hydrogen-bonded complex formed in aqueous solutions of AB. After the same laser irradiation as that for dioxane solution, c-BN NPs were obtained in pyridine and H_2O, as shown in Figure S9a,c. The statistical particle sizes in these two solvents are nearly same with that in dioxane (Figure S9b,d). In contrast, no product was found in cyclohexane solution after the same laser irradiation.

On the basis of above results, we propose a possible mechanism of photochemical synthesis of c-BN NPs. After AB dissolves in dioxane (Scheme 1a), each AB molecule is surrounded by three solvent molecules, forming a basic unit held together by hydrogen bonds (Scheme 1b). As the solution is irradiated by the nanosecond laser with wavelength of 1064 nm (single photon energy 1.165 eV), the four molecules in a basic unit can capture four photons with a total energy of 4.66 eV simultaneously (Scheme 1c). It is possible that the energy is transferred to the central AB molecule through the hydrogen bonds, focuses on a N−H bond (dissociation energy 4.515 eV) or a B−H bond (dissociation energy 3.425 eV),[14] and breaks the bond to release a hydrogen atom (Scheme 1d). Although the above process is a low probability event, it can occur continuously under the intense laser irradiation, noticing the photon flux density is as high as $4.617 \times 10^{28} \text{ cm}^{-2} \text{ s}^{-1}$ (see details in Part S8 of the Supporting Information). Thus, all N−H and B−H bonds in an AB molecule can be broken during a laser pulse, leading to the formation of a BN species (Scheme 1e). Next, the BN species connect into nanoparticles whose structure depends on the laser intensity (Scheme 1f). Under the high-flux laser irradi-

○ H ● B ● C ● N ● O ▪▪▪ Hydrogen Bond
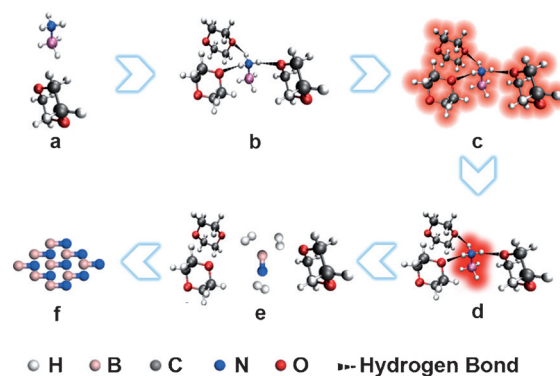
Scheme 1. Formation of c-BN NPs by the dehydrogenation of AB under laser irradiation. For details see text.

ation, a large amount of BN species can be produced, leading to burst nucleation of many fine nanoparticles with narrow size distribution according to LaMer model.[15] The NP size is smaller than the threshold value for stabilizing cubic phase, giving rise to c-BN NPs. In contrast, under low-flux laser a low concentration of BN species is generated, these aggregate into large BN NPs with sizes more than 10 nm. Since the NP sizes exceed the threshold value, the stable structure of the large NPs should be the hexagonal phase. However, the system cannot provide enough driving force for crystallization owing to the large size of NPs and the low synthetic temperature, thus the NPs form an amorphous structure which further transforms into the hexagonal phase under the electron irradiation in TEM.

In summary, we demonstrated that the nanosecond laser irradiation can decompose AB molecules completely for the production of ultrafine c-BN NPs as well as H_2 gas. One AB molecule can combine with three solvent molecules (such as dioxane, pyridine, or water) to form a basic unit, which absorbs four photons at one time, the total energy is high enough to break the chemical bonds in the AB molecules, and generate a local area with a high concentration of BN species, initiating the "burst nucleation" of c-BN NPs. Our findings suggest that the nanosecond laser irradiation is a promising strategy towards superhard materials and hydrogen generation.

Experimental Section

Synthesis of AB: AB was synthesized through the free-radical polymerization of methyl acrylate according to a literature method.[16] In a typical synthesis, ammonium tetrafluoroborate (0.1 mol) and sodium borohydride (0.1 mol) were dissolved in dioxane (500 mL) at room temperature. Then, the mixture solution was heated under reflux overnight at 40 °C after removing oxygen by N_2 flow. Upon completion, the solution was filtered. The filtrate was rotated and evaporated at 70 °C to obtain AB.

Synthesis of c-BN: In a typical experiment, AB (0.03 g) was dissolved in dioxane (10 mL) and dispersed in cyclohexane (10 mL) by sonication, then the solution was irradiated under a nanosecond or millisecond pulsed Nd:YAG laser (1064 nm) for 10 min. The working voltage of the nanosecond laser was fixed at 510, 600, and 700 V. The laser frequency, power density, working current, pulse width and irradiation time for the millisecond laser ablation experiments were set as 10 Hz, 106 $W\,cm^{-2}$, 200 A, 10 ms and 5 min, respectively.

Characterization: The morphology and structure were determined by TEM (FEI Technai G2 F20) equipped with a field emission gun and an EDS unit. Absorption spectra were recorded in a Hitachi U-3010 spectrometer. The luminescence was measured by a Hitachi F-4500 spectrometer. XRD patterns were collected in a Rigaku D/max 2500v/pc diffractometer. FTIR analysis was performed by using a Bruker Tensor 27 spectrometer. EELS was obtained in Gatan Tridiem 863 system.

Calculation method: Density functional theory calculations were carried out at the M06-2X/6-31 + G(d,p) level by using the GAMESS package.[17] The optimized structure was visualized with the aid of the CYLview software.[18]

[1] a) V. L. Solozhenko, O. O. Kurakevych, Y. Le Godec, *Adv. Mater.* **2012**, *24*, 1540–1544; b) I. A. Petrusha, *Diamond Relat. Mater.* **2000**, *9*, 1487–1493; c) S. N. Dub, I. A. Petrusha, *High Pressure Res.* **2006**, *26*, 71–77; d) H. Sumiya, S. Uesaka, S. Satoh, *J. Mater. Sci.* **2000**, *35*, 1181–1186; e) Y. Tian, B. Xu, D. Yu, Y. Ma, Y. Wang, Y. Jiang, W. Hu, C. Tang, Y. Gao, K. Luo, Z. Zhao, L.-M. Wang, B. Wen, J. He, Z. Liu, *Nature* **2013**, *493*, 385–388.

[2] J. Y. Huang, Y. T. Zhu, *Chem. Mater.* **2002**, *14*, 1873–1878.

[3] a) X. P. Hao, D. L. Cui, G. X. Shi, Y. Q. Yin, X. G. Xu, J. Y. Wang, M. H. Jiang, X. W. Xu, Y. P. Li, B. Q. Sun, *Chem. Mater.* **2001**, *13*, 2457–2459; b) J. B. Wang, G. W. Yang, C. Y. Zhang, X. L. Zhong, Z. A. Ren, *Chem. Phys. Lett.* **2003**, *367*, 10–14; c) S. Dong, M. Yu, X. Hao, D. Cui, Q. Wang, K. Li, M. Jiang, *J. Cryst. Growth* **2003**, *254*, 229–234; d) N. Dubrovinskaia, V. L. Solozhenko, N. Miyajima, V. Dmitriev, O. O. Kurakevych, L. Dubrovinsky, *Appl. Phys. Lett.* **2007**, *90*, 101912.

[4] a) D. V. Fedoseev, I. G. Varshavskaya, A. V. Lavrent'ev, B. V. Deryaguin, *Powder Technol.* **1985**, *44*, 125–129; b) L.-L. Zhao, Z.-M. Gao, H. Liu, J. Yang, S.-Z. Qiao, X.-W. Du, *CrystEngComm* **2013**, *15*, 1685–1688; c) S. Z. Mortazavi, P. Parvin, A. Reyhani, R. Malekfar, S. Mirershadi, *RSC Adv.* **2013**, *3*, 1397–1409.

[5] a) H. Zeng, X.-W. Du, S. C. Singh, S. A. Kulinich, S. Yang, J. He, W. Cai, *Adv. Funct. Mater.* **2012**, *22*, 1333–1353; b) K. Kurihara, J. Kizling, P. Stenius, J. H. Fendler, *J. Am. Chem. Soc.* **1983**, *105*, 2574–2579.

[6] F. Lin, J. Yang, S.-H. Lu, K.-Y. Niu, Y. Liu, J. Sun, X.-W. Du, *J. Mater. Chem.* **2010**, *20*, 1103–1106.

[7] J. Yang, T. Ling, W.-T. Wu, H. Liu, M.-R. Gao, C. Ling, L. Li, X.-W. Du, *Nat. Commun.* **2013**, *4*, 1695–1700.

[8] T. Salminen, M. Honkanen, T. Niemi, *Phys. Chem. Chem. Phys.* **2013**, *15*, 3047–3051.

[9] a) K. Y. Niu, J. Yang, S. A. Kulinich, J. Sun, H. Li, X. W. Du, *J. Am. Chem. Soc.* **2010**, *132*, 9814–9819; b) P. Liu, Y. L. Cao, C. X. Wang, X. Y. Chen, G. W. Yang, *Nano Lett.* **2008**, *8*, 2570–2575; c) V. Amendola, M. Meneghetti, *Phys. Chem. Chem. Phys.* **2013**, *15*, 3027–3046.

[10] S. Frueh, R. Kellett, C. Mallery, T. Molter, W. S. Willis, C. King'ondu, S. L. Suib, *Inorg. Chem.* **2011**, *50*, 783–792.

[11] a) K. Watanabe, T. Taniguchi, H. Kanda, *Nat. Mater.* **2004**, *3*, 404–409; b) V. V. Lopatin, F. V. Konusov, *J. Phys. Chem. Solids* **1992**, *53*, 847–854; c) Y. Kubota, K. Watanabe, O. Tsuda, T. Taniguchi, *Science* **2007**, *317*, 932–934; d) K. Watanabe, T. Taniguchi, T. Kuroda, H. Kanda, *Appl. Phys. Lett.* **2006**, *89*, 141902.

[12] a) S. Hu, J. Yang, W. Liu, Y. Dong, S. Cao, J. Liu, *J. Solid State Chem.* **2011**, *184*, 1598–1602; b) C. X. Wang, Y. H. Yang, Q. X. Liu, G. W. Yang, *J. Phys. Chem. B* **2004**, *108*, 728–731.

[13] H. Zeng, S. Yang, W. Cai, *J. Phys. Chem. C* **2011**, *115*, 5038–5043.

[14] J. A. Dean, *Lange's Handbook of Chemistry*, 15th ed., McGraw-Hill, New York, 1999.

[15] a) V. K. L. Mer, *Ind. Eng. Chem.* **1952**, *44*, 1270–1277; b) V. K. LaMer, R. H. Dinegar, *J. Am. Chem. Soc.* **1950**, *72*, 4847–4854.

[16] P. V. Ramachandran, P. D. Gagare, *Inorg. Chem.* **2007**, *46*, 7810–7817.

[17] a) Y. Zhao, D. G. Truhlar, *Theor. Chem. Acc.* **2008**, *120*, 215–241; b) M. W. Schmidt, K. K. Baldridge, J. A. Boatz, S. T. Elbert, M. S. Gordon, J. H. Jensen, S. Koseki, N. Matsunaga, K. A. Nguyen, S. Su, T. L. Windus, M. Dupuis, J. A. Montgomery, Jr., *J. Comput. Chem.* **1993**, *14*, 1347–1363.

[18] CYLview, 1.0b; C. Y. Legault, Université de Sherbrooke, 2009 (http://www.cylview.org).